



Effect of substituents on the aggregate structure and photovoltaic property of violanthrone derivatives

Minmin Shi, Feng Hao, Lijian Zuo, Yi Chen, Yaxiong Nan, Hongzheng Chen*

MOE Key Laboratory of Macromolecule Synthesis and Functionalization, State Key Lab of Silicon Materials, Department of Polymer Science and Engineering, Zhejiang University, Hangzhou 310027, PR China

ARTICLE INFO

Article history:

Received 31 January 2012

Received in revised form

4 May 2012

Accepted 8 May 2012

Available online 15 May 2012

Keywords:

Violanthrone derivatives

Substituent

Aggregate structure

Hole mobility

Organic solar cells

Photovoltaic performance

ABSTRACT

In this paper, three violanthrone derivatives with different substituents, 16,17-bis(2-ethylhexyloxy)-anthra[9,1,2-*cde*]-benzo[*rst*]pentaphene-5,10-dione (**3**), 16,17-bis(octyloxy)-anthra[9,1,2-*cde*]-benzo[*rst*]pentaphene-5,10-dione (**4**), 16,17-bis(hexyloxy)-anthra[9,1,2-*cde*]-benzo[*rst*]pentaphene-5,10-dione (**5**), are synthesized. It is found that the substituent has a great effect on the aggregate structures of violanthrone derivatives: the shorter the side chain is, the stronger the intermolecular π - π actions in the solid state is. Because all compounds are p-type semiconductive materials with the relatively low-lying highest occupied molecular orbital (HOMO) energy levels (~ -5.1 eV) and low band gaps (~ 1.8 eV), their photovoltaic properties are evaluated when the blends of violanthrone derivatives and [6,6]-phenyl-C₆₁-butyric acid methyl ester (PCBM) (1:1, w/w) are used as the active layers of organic solar cells. Among three violanthrone derivatives, compound **5** exhibits the best photovoltaic performance with the power conversion efficiency (PCE) of 0.54% since the aggregate structure of compound **5** is in favor of charge transport.

© 2012 Elsevier Ltd. All rights reserved.

1. Introduction

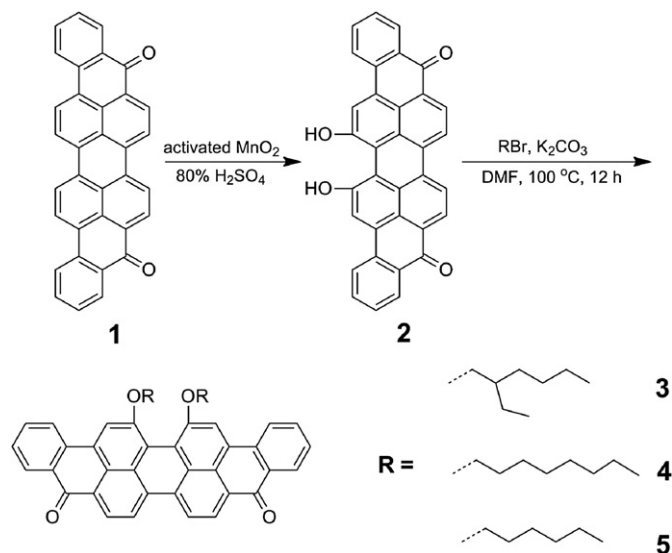
Organic solar cells (OSCs) is regarded as an alternative technology to inorganic photovoltaics because they can be fabricated to large-area and flexible devices by low-cost solution-processing [1–3]. In contrast to inorganic p–n junction solar cells, typical OSCs feature a structure of bulk heterojunction, where a p-type organic semiconductor (either conjugated polymer or small molecule, which is usually a derivative of dye or pigment) and a fullerene derivative (e.g. [6,6]-phenyl-C₆₁-butyric acid methyl ester, abbreviated as PCBM) function as the electron donor and acceptor, respectively. To achieve a higher power conversion efficiency (PCE) of OSCs, an ideal p-type organic semiconductor should own both low band gap (E_g) and low HOMO (highest occupied molecular orbital) energy level: low E_g will favor the efficient harvest of solar photons at longer wavelengths, giving a larger short circuit current (I_{SC}) of OSCs; and low HOMO energy level can increase the open circuit voltage (V_{OC}) of OSCs since V_{OC} is proportional to the difference between the HOMO of the donor and the LUMO (lowest unoccupied molecular orbital) of the

acceptor [4,5]. To meet the above requirements, in the past five years, a lot of new p-type conjugated polymers have been reported, and the best OSCs based on conjugated polymers show the PCEs of more than 8% [6–10]. Unfortunately, in the same period, although significant progresses have been made and the PCEs of $\sim 5\%$ are achieved [11–16], the development of the OSCs based on organic small molecule semiconductors still lags behind the polymer-based counterparts.

Almost all of organic small molecule photovoltaic materials are the derivatives of dyes and pigments. Perylene diimide (PDI) is a typical example. Because of its high electron affinity and excellent electron mobility [17,18], PDI is usually functioned as the electron acceptor in OSCs. Nevertheless, the PCEs of the resulting devices are low, which may be ascribed to the poor morphology of the active layer composed of PDI and p-type organic semiconductor [19,20]. Interestingly, with similar chemical structure as PDI, violanthrone (compound **1**, whose structure is shown in Scheme 1) is a p-type semiconductor because it owns only two carbonyl groups. More importantly, due to its bigger π -conjugated system, violanthrone has a narrower band gap than PDI, so that the absorption band of violanthrone extends to near-infrared region [21]. And it can be also predicted that the HOMO energy level of violanthrone is low because of the electron-accepting ability of two carbonyl groups,

* Corresponding author. Tel./fax: +86 571 8795 2557.

E-mail address: hzchen@zju.edu.cn (H. Chen).



Scheme 1. Synthetic route to compounds 3–5.

which would be in favor of the improvement of V_{OC} while violanthrone is applied as electron donor in OSCs. Therefore, in this work, three soluble violanthrone derivatives with different substituents, 16,17-bis(2-ethylhexyloxy)-anthra[9,1,2-*cde*]-benzo[*rst*]pentaphene-5,10-dione (**3**), 16,17-bis(octyloxy)-anthra[9,1,2-*cde*]-benzo[*rst*]pentaphene-5,10-dione (**4**), 16,17-bis(hexyloxy)-anthra[9,1,2-*cde*]-benzo[*rst*]pentaphene-5,10-dione (**5**), are designed and synthesized. Then, the effects of substituents on the aggregate structures and hole mobilities of compounds **3–5** are investigated. At last, bulk heterojunction OSCs based on the blends of **3–5** and PCBM are fabricated, in order to clarify how the substituents influence the photovoltaic property of violanthrone derivatives through the changing of their aggregate structures.

2. Experimental

2.1. Instrument

^1H NMR and ^{13}C NMR spectra were recorded on a Bruker Avance DMX 300 (300 MHz) nuclear magnetic resonance spectroscope using tetramethylsilane (TMS) as an internal standard. Elemental analysis was conducted on a Perkin–Elmer 240C elemental analyzer. Ultraviolet–visible (UV–Vis) absorption spectra were

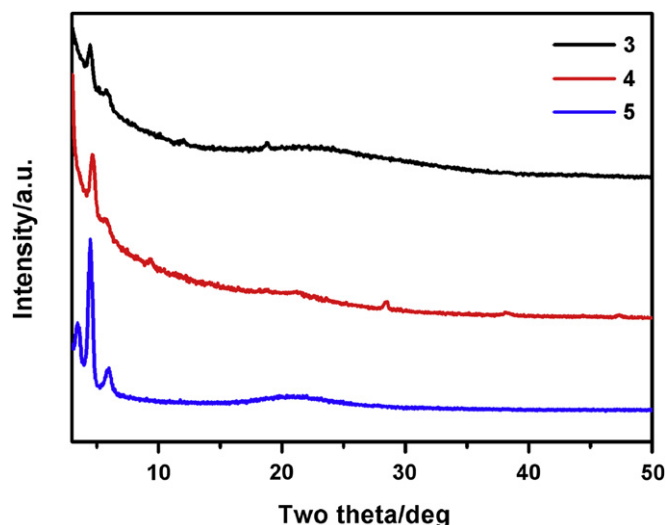


Fig. 2. XRD patterns of the thin films of **3–5** spin-coated on the OTS-modified SiO_2/Si substrates. The spinning speeds are 1000 (**3**) and 2000 rpm (**4** and **5**), respectively.

recorded on a Varian CARY Bio spectrophotometer. Cyclic voltammetry (CV) was done on a CHI 660C electrochemical workstation with Pt plate coated by an organic semiconductive thin film, Pt wire, and standard calomel electrode (SCE) as working electrode, counter electrode, and reference electrode, respectively, in a 0.1 mol/L tetrabutylammonium hexafluorophosphate (Bu_4NPF_6) CH_3CN solution. The redox potentials were measured versus the ferrocene/ferrocenium redox couple (Fc/Fc^+), used as the internal reference. The organic film on the working electrode was formed by casting a solution of compound **3**, **4**, or **5** in chloroform (~ 1 mg/mL). X-ray diffraction (XRD) patterns were gotten on a Rigaku D/max 2550PC X-ray diffractometer with $\text{Cu } K_\alpha$ radiation ($\lambda = 1.5406 \text{ \AA}$) operated at 40 keV and 40 mA. Topographic images of the films were obtained on a Veeco MultiMode atomic force microscopy (AFM) in the tapping mode using an etched silicon cantilever at a nominal load of ~ 2 nN, and the scanning rate for a $10 \mu\text{m} \times 10 \mu\text{m}$ image size was 1.5 Hz.

2.2. Materials

Violanthrone (**1**) was purchased from Huangshan Huafeng Biological Technology Co., PCBM from Sigma–Aldrich Co., and other reagents were commercially available (A.R.) and used as received, unless stated otherwise. All the solvents were freshly distilled prior to use.

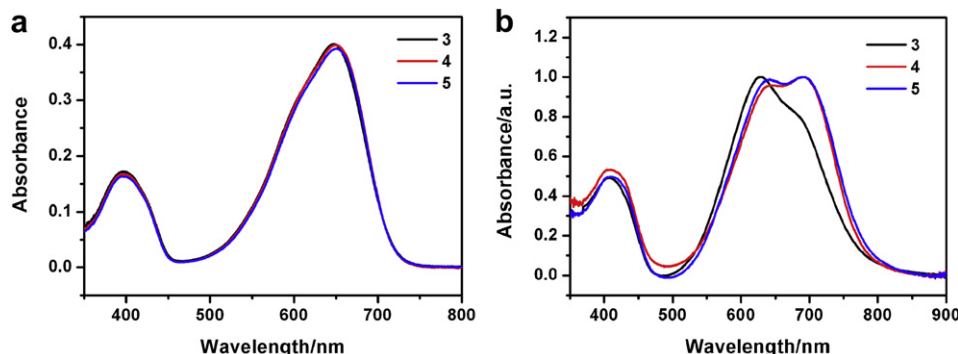


Fig. 1. UV–Vis absorption spectra of the violanthrone derivatives **3–5**: (a) CHCl_3 solutions ($1.00 \times 10^{-5} \text{ M}$) and (b) thin films (~ 80 nm thick).

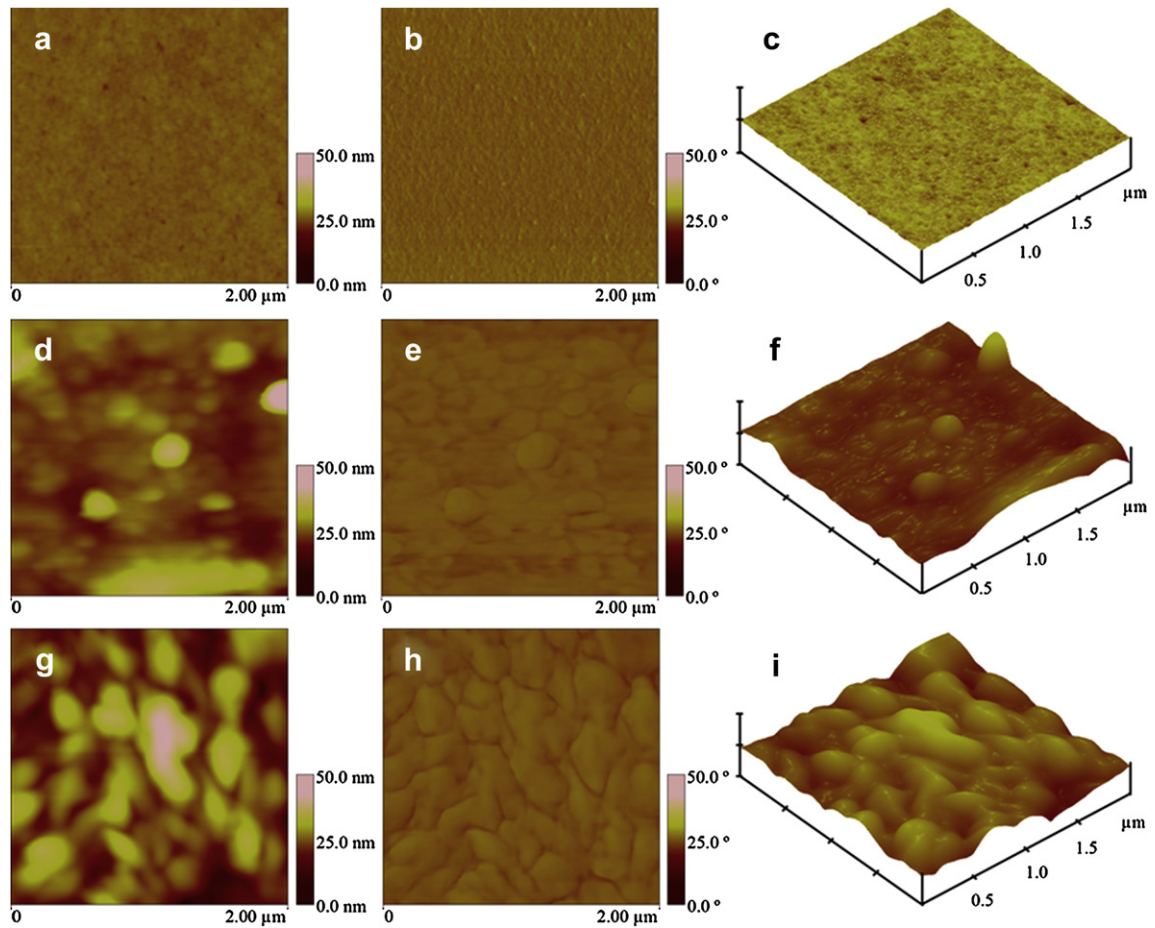


Fig. 3. AFM height (a, d, g), phase (b, e, h), and 3D (c, f, i) images of the thin films of **3** (a, b, c), **4** (d, e, f), and **5** (g, h, i) spin-coated on the OTS-modified SiO₂/Si substrates. The spinning speeds are 1000 (**3**) and 2000 rpm (**4** and **5**), respectively.

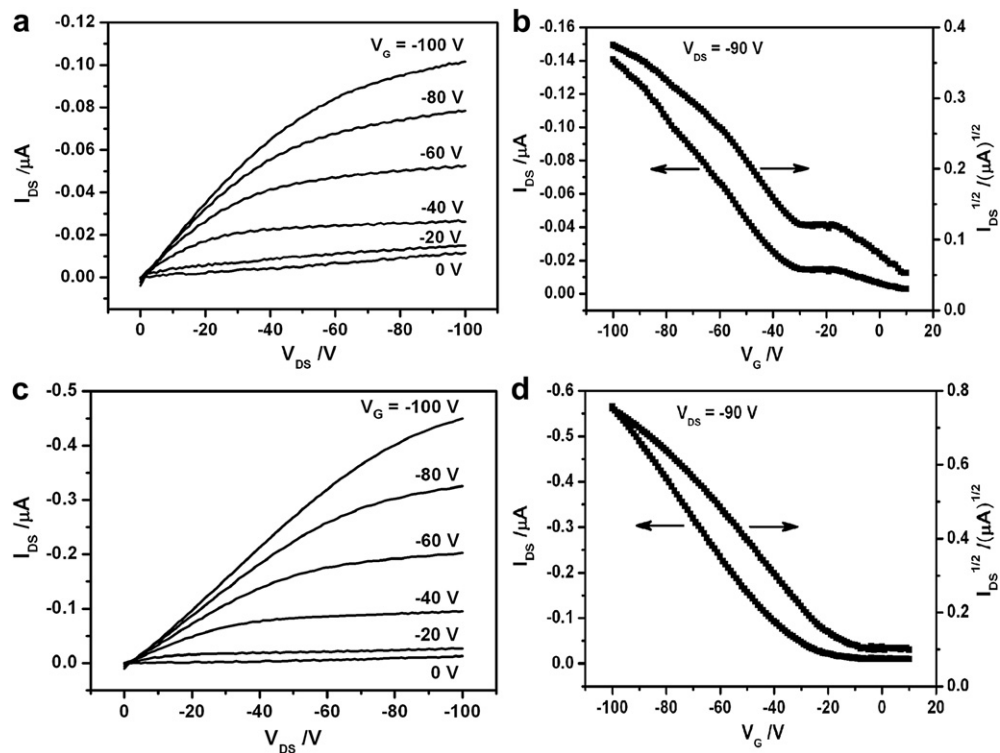


Fig. 4. Output (a, c) and transfer (b, d) characteristics of OFETs based on **4** (a, b) and **5** (c, d) films.

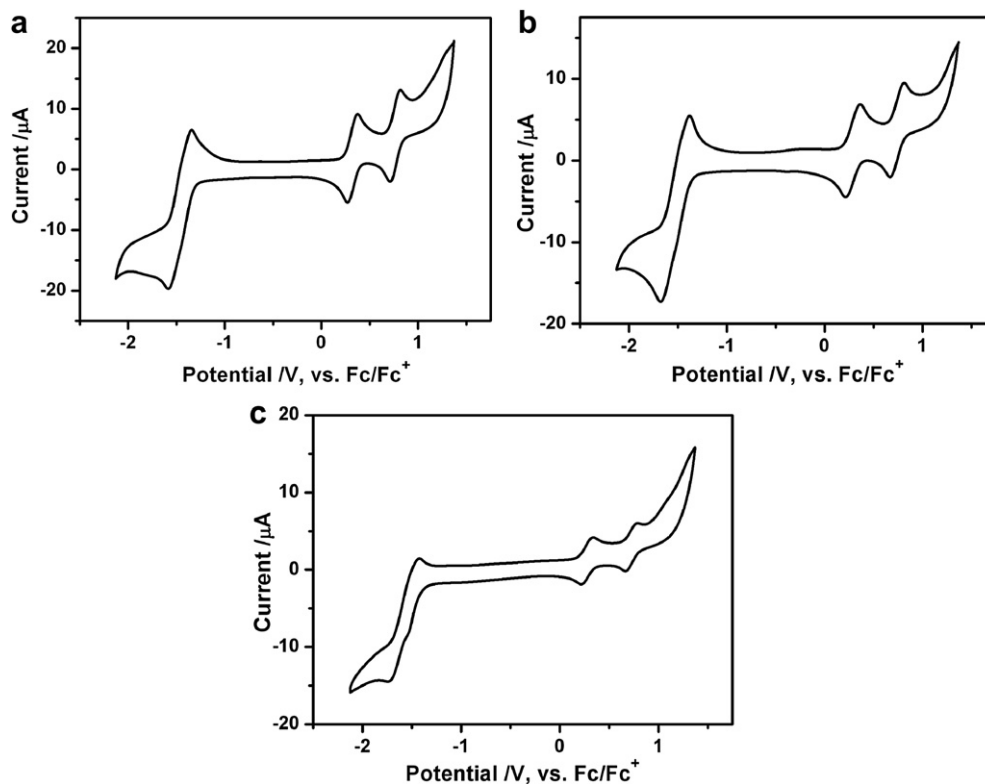


Fig. 5. Cyclic voltammograms of **3** (a), **4** (b), and **5** (c) films coated on platinum plates with the scanning rate of 50 mV/s.

2.3. Synthesis

Target violanthrone derivatives **3–5** were synthesized according to the reported procedure [21], which is outlined in Scheme 1.

3: UV–Vis (CHCl_3): λ_{max} (ϵ) = 648 nm (40,100). ^1H NMR (300 MHz, CDCl_3): δ = 8.80 (d, 2H), 8.65 (d, 2H), 8.57 (d, 2H), 8.41 (d, 2H), 8.30 (s, 2H), 7.83 (t, 2H), 7.62 (t, 2H), 3.92–4.18 (m, 4H), 1.69–1.85 (m, 2H), 1.09–1.61 (m, 16H), 0.67–0.96 (m, 12H). ^{13}C NMR (300 MHz, CDCl_3): δ = 182.88 (s), 156.76 (s), 135.41 (s), 134.09 (s), 133.09 (s), 130.79 (s), 129.14 (s), 128.38 (s), 128.07 (s), 127.46 (s), 127.40 (s), 126.79 (s), 123.49 (s), 123.10 (s), 122.33 (s), 117.27 (s), 114.21 (s), 72.93 (d), 40.02 (s), 30.48 (d), 29.45 (d), 23.77 (s), 23.04 (d), 14.05 (s), 11.24 (d). Elem. Anal. Calcd for $\text{C}_{50}\text{H}_{48}\text{O}_4$: C, 84.24; H, 6.79. Found: C, 84.51; H, 6.52.

4: UV–Vis (CHCl_3): λ_{max} (ϵ) = 650.5 nm (39,900). ^1H NMR (300 MHz, CDCl_3): δ = 8.67 (d, 2H), 8.52 (d, 2H), 8.50 (d, 2H), 8.36 (d, 2H), 8.25 (s, 2H), 7.80 (t, 2H), 7.59 (t, 2H), 4.25 (b, 4H), 1.81–1.92 (m, 4H), 1.40–1.51 (m, 4H), 1.15–1.39 (m, 16H), 0.67–0.94 (m, 6H). ^{13}C NMR (300 MHz, CDCl_3): δ = 182.57 (s), 155.75 (s), 135.21 (s), 133.73 (s), 132.92 (s), 130.63 (s), 128.72 (s), 128.26 (s), 127.96 (s), 127.12 (s), 126.95 (s), 126.52 (s), 123.00 (s), 122.93 (s), 122.13 (s), 116.65 (s), 112.74 (s), 69.28 (s), 31.80 (s), 29.82 (s), 29.56 (s), 29.33 (s), 26.06 (s), 22.66 (s), 14.08 (s). Elem. Anal. Calcd. for $\text{C}_{50}\text{H}_{48}\text{O}_4$: C, 84.24; H, 6.79. Found: C, 84.53; H, 6.60.

5: UV–Vis (CHCl_3): λ_{max} (ϵ) = 651.5 nm (39,300). ^1H NMR (300 MHz, CDCl_3): δ = 8.56 (d, 2H), 8.46 (d, 2H), 8.38 (d, 2H), 8.33 (d, 2H), 8.20 (s, 2H), 7.78 (t, 2H), 7.57 (t, 2H), 4.23 (b, 4H), 1.81–1.92 (m, 4H), 1.40–1.52 (m, 4H), 1.23–1.39 (m, 8H), 0.84–0.94 (m, 6H). ^{13}C NMR (300 MHz, CDCl_3): δ = 183.19 (s), 156.29 (s), 135.52 (s), 134.46 (s), 133.14 (s), 130.95 (s), 129.39 (s), 128.49 (s), 128.20 (s), 127.70 (s), 127.44 (s), 127.14 (s), 123.64 (s), 123.14 (s), 122.74 (s), 117.15 (s), 114.23 (s), 69.69 (s), 31.65 (s), 29.79 (s), 25.69 (s), 22.59 (s), 13.99 (s). Elem. Anal. Calcd. for $\text{C}_{46}\text{H}_{40}\text{O}_4$: C, 84.14; H, 6.14. Found: C, 84.31; H, 6.32.

2.4. Organic field-effect transistors (OFETs) fabrication and measurement

OFETs were fabricated in a top-contact configuration on p-doped Si (100) wafers with 200 nm thick thermally grown SiO_2 ($C_i = 10 \text{ nF/cm}^2$). After a normal cleaning procedure with solvents in an ultrasonic bath, Si/ SiO_2 substrates were exposed to octadecyltriethoxysilane (OTS) vapor at room temperature to form a self-assembled monolayer (SAM) of OTS on the surface. Then, a 10 mg/mL solution of compound **3**, **4**, or **5** in chloroform was spin-coated onto the substrates with a spinning speed of 1000 (**3**) or 2000 rpm (**4** and **5**) for 60 s and dried in vacuum until the solvent had evaporated completely, giving an organic semiconductive layer, with a thickness of about 80 nm. Finally, on top of the semi-conducting thin film, Au drain and source electrodes ($\sim 50 \text{ nm}$ thick) were deposited under vacuum through a shadow mask, where the drain-source channel length (L) and width (W) are 50 μm and 2.4 mm, respectively. Current–voltage (I – V) characteristics of the OFET devices were measured in an ambient atmosphere with a Keithley 6430 sub-femtoamperometer (drain) and Keithley 2400 (gate) source meter, operated by a locally written Labview program and GPIB communication. Field-effect mobility (μ) was calculated by the following equation:

$$\mu = (2L/WC_i) \left(\frac{\partial I_{\text{DS}}^{1/2}}{\partial V_G} \right)^2 \quad (1)$$

where I_{DS} was the source-drain current, V_G was the gate voltage, $\partial I_{\text{DS}}^{1/2} / \partial V_G$ was the slope of $I_{\text{DS}}^{1/2}$ versus V_G at the saturation region (V_G , from 0 to -100 V ; V_{DS} , -90 V).

2.5. OSCs fabrication and characterization

OSCs were fabricated with indium tin oxide (ITO) glass as the anode, Al as the cathode, and a blended film of violanthrone

Table 1
Electrochemical properties of violanthrone derivatives 3–5.

Compound	E_{ox} (V)	HOMO (eV)	E_{red} (V)	LUMO (eV)	E_g^{ec} (eV)
3	0.33	-5.13	-1.46	-3.34	1.79
4	0.29	-5.09	-1.52	-3.28	1.81
5	0.28	-5.08	-1.53	-3.27	1.81

derivative:PCBM between the two electrodes as the photoactive layer. The ITO glass was pre-cleaned and PEDOT:PSS [poly(3,4-ethylenedioxythiophene):poly(styrenesulfonate)] (Baytron P 4083, Germany) was spin-coated at 3000 rpm for 60 s on the ITO substrate. The thickness of the PEDOT:PSS layer was about 30 nm. Then, a 20 mg/mL solution of violanthrone derivative and PCBM (1:1, w/w) in $CHCl_3$ was spin-coated at 1000 rpm for 30 s onto the PEDOT:PSS layer. The thickness of the photoactive layer is in the range 80–100 nm (calibrated by an Ambios Technology XP-2 profilometer). At last, a 100 nm thick Al film was deposited on the photoactive layer under vacuum of $\sim 4 \times 10^{-4}$ Pa. The active area of OSCs was 9 mm². I - V characteristics of the devices in the dark and under illumination were recorded on a semiconductor parameter analyzer (Keithley 2400-SCS). A Thermal Oriel solar simulator was used to give AM 1.5G irradiance of 100 mW/cm². The input photon to converted current efficiency (IPCE) was measured using an 8300 lock-in amplifier unit coupled with a WDG3 monochromator and a 500 W Xenon lamp.

3. Results and discussion

Fig. 1 shows the UV–Vis absorption spectra of compounds 3–5 in $CHCl_3$ solutions and in thin films. It is found that each solution presents the nearly same absorption bands (Fig. 1a), implying that the substituents have neglectable effects on the frontier orbitals of violanthrone derivatives. However, different alkyl side chains can influence greatly the aggregation behaviors of violanthrone derivatives. From Fig. 1b, it is observed that, due to the intermolecular π - π overlapping in the condensed state, the thin films of violanthrone derivatives exhibit an additional absorption peak centered at around 690 nm, and the absorption intensities of compounds 4 and 5 are obviously stronger than that of compound 3. This phenomenon is reasonable that the branched alkyl group,

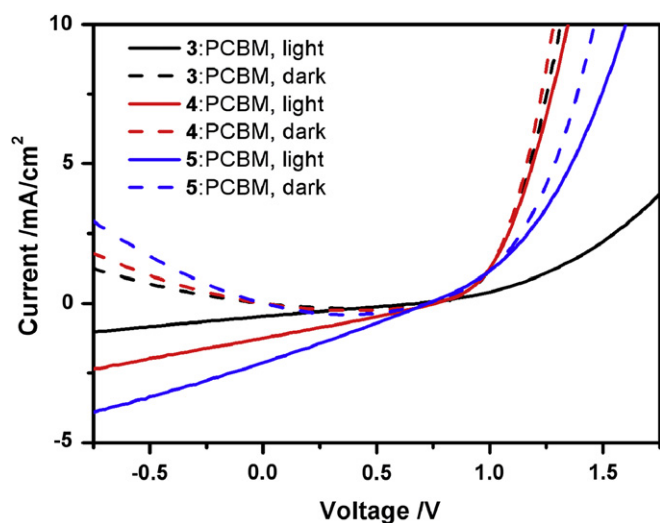


Fig. 6. I - V characteristics of the OSCs with the violanthrone derivative:PCBM blends as the active layers in dark (dash lines) and under illumination of AM 1.5 G, 100 mW/cm² (solid lines).

Table 2
Photovoltaic performances of the OSCs based on the blends of violanthrone derivatives 3–5 and PCBM.

Active layer	V_{oc} (V)	I_{sc} (mA/cm ²)	FF	PCE (%)
3:PCBM	0.68	0.47	0.29	0.093
4:PCBM	0.76	1.27	0.27	0.26
5:PCBM	0.74	2.14	0.34	0.54

2-ethylhexyl in compound 3 would show bigger steric repulsion than the linear alkyl groups, i.e. octyl in 4 and hexyl in 5, which prevents from effective π - π stacking of successive violanthrone rings in the film of 3.

The hypothesis can be confirmed directly by XRD (Fig. 2) and AFM (Fig. 3) characterizations. As demonstrated in Figs. 2, 4 and 5 films exhibit much stronger XRD peaks than 3 film, suggesting that 4 and 5 films own higher crystallinity although they are prepared with a higher spinning speed (2000 rpm). Among three films, 5-film shows the highest crystallinity, which is ascribed to the smallest steric repulsion of hexyl group. As shown in AFM photographs (Fig. 3), 3-film appears very smooth with a typical root mean square roughness (R_q) of 0.218 nm, indicating that the aggregation of violanthrone molecules is blocked remarkably by the branched side chains. When the side group is changed to linear octyl and hexyl, violanthrone molecules are easier to aggregate via π - π interactions of adjacent chromophores. Therefore, 4 and 5 films consist of aggregates larger than 50 nm. The shorter the side chain is, the bigger the aggregates are, and the rougher the film is.

The performances of OFETs with 4–5 films as the transporting layers also support the above finding. From the OFETs' transfer and output traces (Fig. 4), the hole mobilities of 4 and 5 are calculated as 1.76×10^{-4} and 3.15×10^{-4} cm²V⁻¹s⁻¹, respectively. Instead, the hole mobility of 3 is only 4.93×10^{-5} cm²V⁻¹s⁻¹ [21]. The difference in hole mobility among compounds 3–5 is rationally attributed to their distinguishing aggregate structures. Since the linear side chains in compounds 4 and 5, in particular, hexyl group of compound 5, would be in favor of the intermolecular π - π actions and crystallinity in the solid state, thus, charge carriers are easier to hop from one molecule to nearby molecules. So, compound 5 has the highest hole mobility.

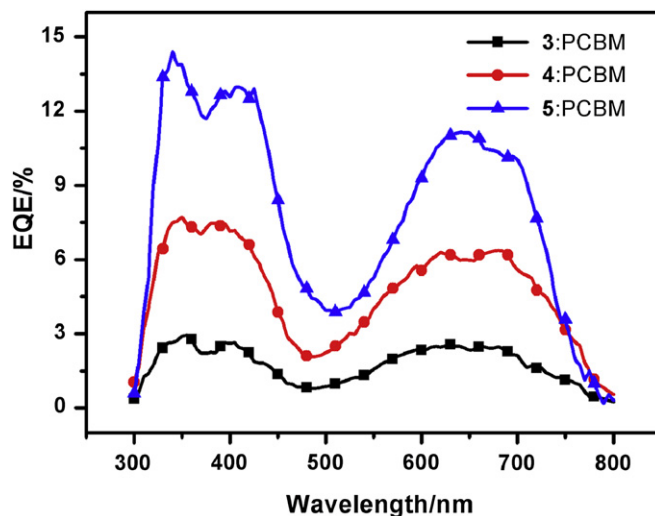


Fig. 7. IPCE curves of the OSCs with the violanthrone derivative:PCBM blends as the active layers.

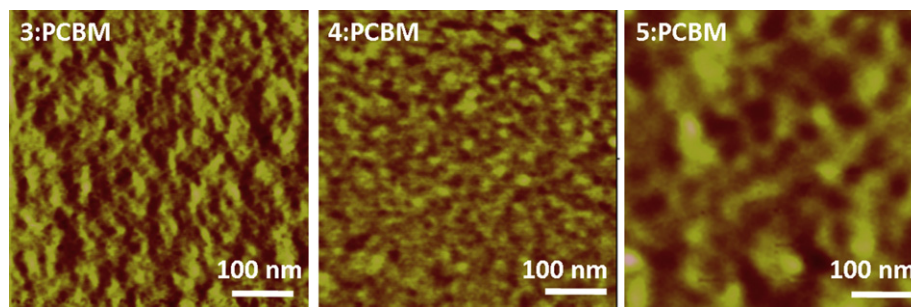


Fig. 8. AFM phase images of violanthrone derivative:PCBM blended films.

Fig. 5 presents cyclic voltammograms (CV) of **3–5** films and their electrochemical data are summarized in Table 1. From Fig. 5, it is found that, three violanthrone derivatives exhibit the same electrochemical behaviors: two couples of quasi-reversible reduction/oxidation peaks in the positive potential region, and a couple of irreversible redox waves in the negative potential range are observed, indicating that all of compounds are typical p-type materials. The onset oxidation potentials (E_{ox}) are 0.33 V versus Fc/Fc⁺ for **3**, 0.29 V versus Fc/Fc⁺ for **4**, and 0.28 V versus Fc/Fc⁺ for **5**, from which the HOMO energy levels of **3**, **4**, and **5** are estimated as -5.13 , -5.09 , and -5.08 eV, respectively, because the absolute energy level of Fc/Fc⁺ is 4.8 eV below vacuum [15]. Similarly, the LUMO energy levels and of **3**, **4**, and **5** can be calculated as -3.34 , -3.28 , and -3.27 eV, respectively, from their onset reduction potentials (E_{red}). Thus, the electrochemical band gaps (E_g^{ec}) are determined as 1.79, 1.81, and 1.81 eV for **3**, **4**, and **5**, respectively. Based on the above data, it can be predicted that compounds **3–5** would be potential electron donors in OSCs since they possess both relatively low-lying HOMO energy levels as well as low band gaps.

In order to evaluate the photovoltaic properties of compounds **3–5**, OSCs were fabricated with the blends of different violanthrone derivatives and PCBM (1:1, w/w) as the active layers. Fig. 6 shows $I-V$ curves of the three OSCs in dark and under the illumination of AM 1.5G solar irradiance (100 mW/cm²). From Fig. 6, their corresponding open circuit voltage (V_{oc}), short circuit current (I_{sc}), fill factor (FF), and power conversion efficiency (PCE) are obtained and summarized in Table 2. It is obviously observed that the OSCs based on three violanthrone derivatives exhibit approximate open circuit voltages (~ 0.7 V), which agrees exactly with the HOMO energy levels of **3–5**. However, three devices give different short circuit currents and follow the sequence: **3** < **4** < **5**, which is consistent with the degrees of the intermolecular $\pi-\pi$ stacking in **3–5** films, because the stronger $\pi-\pi$ interactions favor the transportation of charge carriers in OSCs. Therefore, among three devices, the OSC made from **5**:PCBM blend shows the largest I_{sc} (2.14 mA/cm²) and the highest PCE (0.54%). The external quantum efficiency (EQE) plot of three devices under the short circuit condition is presented in Fig. 7, in which the photocurrent response ranges of the devices are quite broad (300–800 nm), which is in accordance with the absorption spectra of compounds **3–5**. However, the maximum EQE is less than 15%, which can be attributed to large phase-separated domains in the blended films (Fig. 8), suggesting that the morphology of the violanthrone derivative:PCBM blended film needs further optimizations in order to achieve better photovoltaic performance.

4. Conclusion

We synthesize three soluble violanthrone derivatives with different alkyloxy groups, and find that all compounds are p-type

organic semiconductors with the relatively low-lying HOMO energy levels (~ -5.1 eV) and the broad absorption ranges extended to 800 nm, implying that they can be used as electron donors in OSCs. Preliminary photovoltaic study discloses that the violanthrone derivative with the shortest hexyloxy substituent (compound **5**) exhibits the best photovoltaic performance (PCE = 0.54%) because the shortest linear side chain is favor of the intermolecular $\pi-\pi$ actions in the solid state, providing a relatively high hole mobility of 3.15×10^{-4} cm² V⁻¹ s⁻¹. These findings suggest that the appropriate molecular tailoring of some dyestuffs is a simple and feasible route to good organic small molecule photovoltaic materials.

Acknowledgments

This work was supported by the National Natural Science Foundation of China (Nos. 50990063, 51073135, 51011130028). We also would like to gratefully acknowledge support from the National High Technology Research and Development Program of China (863 Program) (No. 2011AA050520).

Appendix A. Supporting information

Supplementary data related to this article can be found online at doi:10.1016/j.dyepig.2012.05.003.

References

- [1] Service RF. Outlook brightens for plastic solar cells. *Science* 2011;332:293.
- [2] Walker B, Kim C, Nguyen TQ. Small molecule solution-processed bulk heterojunction solar cells. *Chem Mater* 2011;23:470–82.
- [3] Günes S, Neugebauer H, Sariciftci NS. Conjugated polymer-based organic solar cells. *Chem Rev* 2007;107:1324–38.
- [4] Scharber MC, Mühlbacher D, Koppe M, Denk P, Waldauf C, Heeger AJ, et al. Design rules for donors in bulk-heterojunction solar cells – towards 10% energy-conversion efficiency. *Adv Mater* 2006;18:789–94.
- [5] Cheng YJ, Yang SH, Hsu CS. Synthesis of conjugated polymers for organic solar cell applications. *Chem Rev* 2009;109:5868–923.
- [6] Li YF. Molecular design of photovoltaic materials for polymer solar cells: toward suitable electronic energy levels and broad absorption. *Acc Chem Res* 2012. doi:10.1021/ar2002446.
- [7] Chen HY, Hou JH, Zhang SQ, Liang YY, Yang GW, Yang Y, et al. Polymer solar cells with enhanced open-circuit voltage and efficiency. *Nat Photonics* 2009;3:649–53.
- [8] He ZC, Zhong CM, Huang X, Wong WY, Wu HB, Chen LW, et al. Simultaneous enhancement of open-circuit voltage, short-circuit current density, and fill factor in polymer solar cells. *Adv Mater* 2011;23:4636–43.
- [9] Huo LJ, Zhang SQ, Guo X, Xu F, Li YF, Hou JH. Replacing alkoxy groups with alkylthienyl groups: a feasible approach to improve the properties of photovoltaic polymers. *Angew Chem Int Ed* 2011;50:9697–702.
- [10] Son HJ, Wang W, Xu T, Liang YY, Wu Y, Li G, et al. Synthesis of fluorinated polythienothiophene-co-benzodithiophenes and effect of fluorination on the photovoltaic properties. *J Am Chem Soc* 2011;133:1885–94.
- [11] Walker B, Tamayo AB, Dang XD, Zalar P, Seo JH, Garcia A, et al. Nanoscale phase separation and high photovoltaic efficiency in solution-processed, small-molecule bulk heterojunction solar cells. *Adv Funct Mater* 2009;9:3063–9.

- [12] Wei GD, Lunt RR, Sun K, Wang SY, Thompson ME, Forrest SR. Efficient, ordered bulk heterojunction nanocrystalline solar cells by annealing of ultrathin squaraine thin films. *Nano Lett* 2010;10:3555–9.
- [13] Zhou JY, Wan XJ, Liu YS, Long GK, Wang F, Li Z, et al. A planar small molecule with dithienosilole core for high efficiency solution-processed organic photovoltaic cells. *Chem Mater* 2011;23:4666–8.
- [14] Matsuo Y, Sato Y, Niinomi T, Soga I, Tanaka H, Nakamura E. Columnar structure in bulk heterojunction in solution-processable three-layered p-i-n organic photovoltaic devices using tetrabenzoporphyrin precursor and silyl-methyl[60]fullerene. *J Am Chem Soc* 2009;131:16048–50.
- [15] Shang HX, Fan HJ, Liu Y, Hu WP, Li YF, Zhan XW. A solution-processable star-shaped molecule for high-performance organic solar cells. *Adv Mater* 2011;23:1554–7.
- [16] Sun YM, Welch GC, Leong WL, Takacs CJ, Bazan GC, Heeger AJ. Solution-processed small-molecule solar cells with 6.7% efficiency. *Nat Mater* 2012;11:44–8.
- [17] Chen HZ, Ling MM, Mo X, Shi MM, Wang M, Bao Z. Air stable n-channel organic semiconductors for thin film transistors based on fluorinated derivatives of perylene diimides. *Chem Mater* 2007;19:816–24.
- [18] Malenfant PRL, Dimitrakopoulos CD, Gelorme JD, Kosbar LL, Graham TO, Curioni A, et al. N-type organic thin-film transistor with high field-effect mobility based on a N, N'-dialkyl-3,4,9,10-perylene tetracarboxylic diimide derivative. *Appl Phys Lett* 2002;80:2517–9.
- [19] Schmidt-Mende L, Fechtenkötter A, Müllen K, Moons E, Friend RH, MacKenzie JD. Self-organized discotic liquid crystals for high-efficiency organic photovoltaics. *Science* 2001;293:1119–22.
- [20] Zhou EJ, Cong JZ, Wei QS, Tajima K, Yang CH, Hashimoto K. All-polymer solar cells from perylene diimide based copolymers: material design and phase separation control. *Angew Chem Int Ed* 2011;50:2799–803.
- [21] Shi MM, Chen Y, Nan YX, Ling J, Zuo LJ, Qiu WM, et al. π - π Interaction among violanthrone molecules: observation, enhancement, and resulting charge transport properties. *J Phys Chem B* 2011;115:618–23.